Deep Level Transient Spectroscopy (DLTS) on Colloidal-Synthesized Nanocrystal Solids

Deniz Bozyigit, Michael Jakob, Olesya Yarema, and Vanessa Wood
Laboratory for Nanoelectronics, Department of Information Technology and Electrical Engineering, Eidgenoessische Technische Hochschule Zurich
(Dated: November 23, 2012)

We demonstrate current-based deep level transient spectroscopy (DLTS) on semiconductor nanocrystal solids to obtain quantitative information on deep-lying trap states, which are know to limit optoelectronic device performance. In particular, our results from a Schottky-type solar cell containing a PbS nanocrystal solid reveal a deep trap with an activation energy of 0.40 eV and a density of $N_T = 1.7 \times 10^{17}\,\mathrm{cm}^{-3}$. We discuss our findings in the context of previously proposed charge transport models for PbS nanocrystal solids.

New semiconductor materials, which can be manufactured by low cost solution based processes, hold promise for next generation electronic and optoelectronic device applications. In particular colloidally synthesized semiconductor nanocrystals (NCs) are of interest, due to their excellent optical properties and the tunability of key material properties, such as their bandgap. To date, a variety of NC material systems have been used to demonstrate field-effect transistors (FETs) [1, 2], LEDs [3], and photovoltaic (PV) cells [4–8]. Although recent reports show relevant performances, e.g. FETs with charge carrier mobilities of $30\,\mathrm{cm}^2/(\mathrm{Vs})$ [2] and solarcells with power conversion efficiencies of 7.4 % [9], performance metrics must increase for commercial application.

It is well established in traditional semiconductor (SC) research that the performance of any SC device is strongly affected by the presence of electronic states within the bandgap. Even in very small concentrations ($\ll$ 1 ppm or $10^{17}\,\mathrm{cm}^{-3}$) such states - or charge carrier traps - can alter the electrical properties of a SC. Their impact on device performance is dependent on the relative position of the traps in the band gap [10, 11]. Traps close to the middle of the band gap act as efficient recombination (or generation) centers, thereby reducing the quantum efficiencies of LED and PV devices. Traps close to the conduction band and valence band however reduce the mobility of free electrons and holes and can act as dopants, changing the Fermi energy. In large concentrations ($>$ 1 ppm or $10^{17}\,\mathrm{cm}^{-3}$), these traps can pin the Fermi energy to a fixed level and thereby alter the formation of SC-SC or SC-metal interfaces.

The significance of trap states on charge transport in NC based devices is rapidly gaining interest [9, 12–15]. Although systematic and quantitative understanding is still lacking, various chemical treatments have been proven to incrementally improve device performance [2, 9, 13] and it is suspected that this is due to the passivation of trap states. Attempts have been made to quantify charge traps in NC solids [9, 16], but the lack of predictive models for charge transport in such materials makes it difficult to interpret the data.

In this work we demonstrate how deep level transient spectroscopy (DLTS) can be used to quantify traps in NC solids. In the past, DLTS has been used very successfully to characterize the density of traps (N_T), the trap energy (E_T), and the capture cross section (σ_T) traps in conventional [17] and organic SCs [18]. As an initial material system, we choose NC solids composed of PbS NCs with an ethanedithiol (EDT) surface treatment since it is commonly used as the active material in a variety of NC solar cells [4–9], and the performance limitations are believed to be linked to the presence of trap states [7].

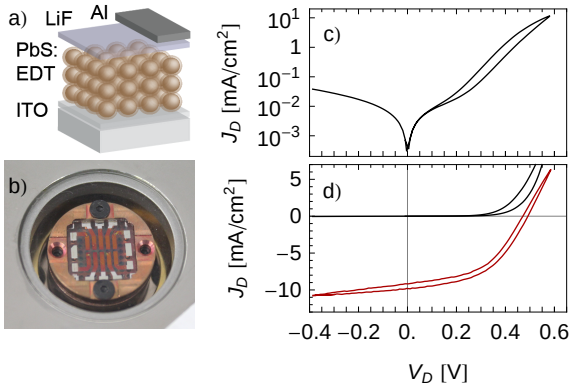

FIG. 1: **a)** Schematic of the Schottky junction solar cell. **b)** Photograph of device in cryostat. **c)** Current-density versus voltage for the solar cell examined in the dark, show a clear diode behaviour with a rectification $>$ 100 and a small hysteresis. **d)** Current-density versus voltage for the solar cell examined in the dark (black line) and under AM1.5G illumination (red line). The device characteristics and power conversion efficiency of 2.3 % are typical of literature values.

The devices used in this study are Schottky diodes made from ITO/PbS:EDT with a LiF/Al cathode - shown schematically in Fig. (1a) which are known to work as solar cells [7, 19]. Our device is fabricated by a layer-by-layer dipcoating technique (See Supplementary Information) and is shown in the photograph in Fig. (1b).

Prior to preforming DLTS measurements, we verify that our devices perform well as a solar cell. Fig. (1c) shows the current density versus voltage characteristics of the device in the dark. We observe a typical diode with a rectification of $>$ 100 and a small hysteresis. Fig. (1d) shows the current density versus voltage characteristics of the solar cell in the dark and under AM1.5G illumination. For the device, which was used for DLTS measurements, we determine a open-circuit voltage (V_{oc}) of 0.47 V, a short-circuit current (J_{sc}) of $9.7\,\mathrm{mA/cm}^2$, a fill-factor of 51 %, and a power conversion efficiency of 2.3 %. These values are comparable to other published device perfor-

mances [7, 19].

DLTS methods are based on the measurement of a transient signal (voltage, capacitance, current, or charge) over a range of temperatures. From the decay dynamics of the transients, DLTS analysis enables extraction of the important trap parameters: the trap density (N_T), the trap activation energy (ΔE_T), and the trap capture cross section (σ_T). In the initial demonstrations of DLTS by Lang et al., capacitance transients were measured to extract this information [20]. In such an experiment, the space charge region (SCR) acts as a transducer between the charge in the traps and the measured SCR-capacitance. While this transducer effect can be advantageous, it requires a detailed understanding of the SCR. In particular it is known that large trap densities invalidate the underlying assumptions necessary for capacitance-based DLTS [17]. This may be the reason, why earlier attempts of DLTS on NC materials did not yield conclusive results about trap state densities and energies [16].

We turn to a current-based DLTS method [21] (often refered to as Q-DLTS), which employs the measurement of current transients and was particularly successful for organic materials [18, 22]. We perform the current transient measurements using the experimental setup depicted in Fig. (2a). Using an arbitrary waveform generator (Agilent 33522A), we apply a reverse bias ($V_\mathrm{D} = -0.7\,\mathrm{V}$) to the device and a voltage pulse every 10 ms for 1 ms as shown in Fig. (2c). Simultaneously, the current density through the device ($J_\mathrm{D}(t)$) is measured using a broadband low current amplifier (FEMTO DHPCA-100) connected to an oscilloscope (R&S RTM1054).

During the forward section of the pulse ($V_\mathrm{D} = 0\,\mathrm{V}$), traps in the SCR can be populated (Fig. (2b), top). At time $t = 0$, when the reverse bias is again applied, the populated traps can emit the captured charge carriers so as to thermalize to the new bias condition. This carrier emission process is observed as a current transient in the device current signal (Fig. (2d)). However, in addition to the current due to trap emission (J_E), in which we are interested, the capacitive displacement current (J_cap) and the reverse leakage current (J_leak), also contribute to the total measured device current (J_D):

$$J_\mathrm{D}(t) = J_\mathrm{E}(t) + J_\mathrm{cap}(t) + J_\mathrm{leak}. \tag{1}$$

To eliminate the contribution of J_leak, we subtract the baseline of the measured current (at 8 ms). Further, we estimate the displacement current by $J_\mathrm{cap,est}(t) = C_{1\,\mathrm{MHz}} \frac{dV_\mathrm{D}}{dt}$. We independently measure the high frequency capacitance $C_{1\,\mathrm{MHz}} = 225\,\mathrm{nF/cm^2}$ using an impedance analyzer (SOLARTRON MODULAB MTS). Based on this estimation, we choose a starting time t_0 for the trap emission transients such that $J_\mathrm{cap,est}(t_0) \ll J_\mathrm{E}(t_0)$. Thus, we obtain the transients of the trap emission current $J_\mathrm{E}(t)$ plotted in Fig. (2e), which were recorded for sample temperatures of $131 - 299\,\mathrm{K}$.

Based on the Shockley-Read-Hall (SRH) model, the current originating from emitting traps is given by

$$J_\mathrm{E}(t) = \sum_i \frac{W N_{\mathrm{T},i}}{\tau_\mathrm{E,i}} \exp\left(-\frac{t}{\tau_\mathrm{E,i}}\right), \tag{2}$$

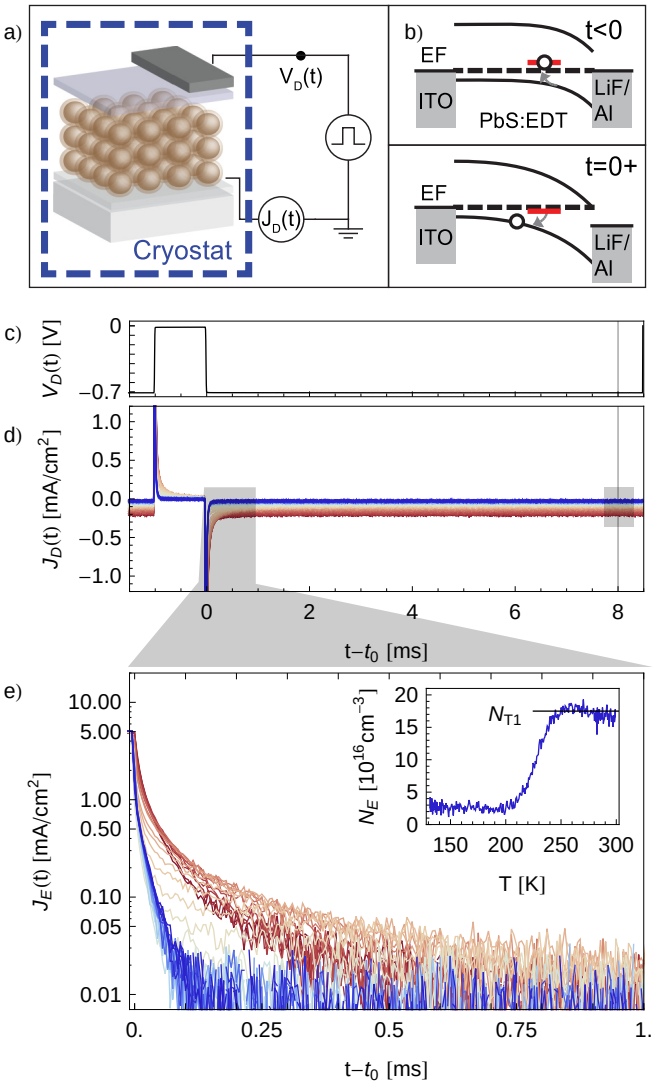

FIG. 2: **a)** Schematic of the DLTS measurement setup. Voltage pulses (V_D) are applied to the diode while the current density (J_D) is measured. **b)** Schematic of the band diagrams before ($t < 0$) and after ($t = 0^+$) the voltage step. After the step, previously occupied traps adjust to the new bias condition by emitting carriers that can be measured as a current transient. **c)** Time trace of the voltage applied to the device (V_D). **d)** Measurement of the current through the device (J_D) for temperatures between 131 K (blue) to 300 K (red). The current value at $t = 8$ ms is used to estimate the leakage current (J_leak). **e)** Transients of the trap emission current (J_E). The inset shows the total density of emitted carriers (N_E) calculated from J_E. Close to room temperature, we find a constant number of emitted carriers, $N_{\mathrm{T}1} = 1.7 \times 10^{17}\,\mathrm{cm^{-3}}$.

where W is the width of the SCR, $N_{\mathrm{T},i}$ is the volume density, and $\tau_\mathrm{E,i}$ is the emission time constant for a trap of type i. Assuming that charge carrier emission is a thermally activated process, the emission time constant for each trap type i is given by

$$\tau_\mathrm{E,i} = \sigma_{\mathrm{T},i} \Gamma_{p(n)} T^{-2} \exp\left(-\frac{\Delta E_{\mathrm{T},i}}{kT}\right), \tag{3}$$

where $\sigma_\mathrm{T,i}$ is the cross-section of the trap, $\Delta E_{\mathrm{T},i}$ is the

activation energy of the trap to a transporting band, k the Boltzmann constant, and T the temperature of the system. The material dependent factor $\Gamma_{p(n)}$ is given by

$$\Gamma_{p(n)} = 2 \times 3^{1/2}(2\pi/h^2)^{3/2}k^2 m^*_{p(n)} \quad (4)$$
$$= 3.256 \times 10^{20}\,\mathrm{K^{-2}cm^{-2}s^{-1}}, \quad (5)$$

where h is the Planck constant based on the effective mass of the free holes (and electrons) $m^*_{p(n)} = 0.1m_e$ in bulk PbS [23]. Due to the exponential temperature dependence, long emission time constants can achieved at low temperatures, such that traps effectively *freeze out*, i.e. are prevented from being (de)populated in the time window of observation.

Based on Eq. (2), the total density of emitted carriers (N_E) can be determined by integrating the measured J_E:

$$N_\mathrm{E} = \frac{1}{Wq}\int J_\mathrm{E}(t)dt = \sum_i N_{\mathrm{T},i}, \quad (6)$$

where q is the electron charge. We perform this integration for each transient, and, in Fig. (2f), plot the result versus the temperature at which the current transient is taken. In this plot of emitted carrier density versus temperature, two regions can be clearly distinguished. At 300 K, a trap density of $N_{\mathrm{T},1} = 1.7 \times 10^{17}\,\mathrm{cm^{-3}}$ is measured. These traps start to freeze out at 250 K such that below 200 K, only a residual charge density of $3 \times 10^{16}\,\mathrm{cm^{-3}}$ is observed.

We can now use the same current transient data to extract the trap activation energy (ΔE_T) and the crossection (σ_T) by calculating the DLTS spectrum (ΔQ):

$$\Delta Q = Q(t_2) - Q(t_1) = \int_{t_1}^{t_2} J_\mathrm{E}(t)dt, \quad (7)$$

where t_1, t_2 are two times that can be freely chosen to define a detector time constant (τ_Q) given by

$$\tau_\mathrm{Q} = \frac{t_2 - t_1}{\log t_2/t_1}. \quad (8)$$

It is at the core of the DLTS technique that ΔQ is most sensitive to transients with emission time constants similar to τ_Q, while other transients with longer or shorter time constants have little influence on the spectrum. In Fig. (3a) we plot ΔQ vs temperature for a fixed ratio $t_2/t_1 = 5$ and τ_Q between 10 μs and 1 ms. A peak appears at the temperatures where the trap emission time τ_E becomes equal to τ_Q. Plotting the peak temperatures in an Arrhenius-type plot as $\log(\tau_\mathrm{Q}T^2)$ vs $1000/T$ in Fig. (3b) we find a linear dependence and can extract an activation energy of $\Delta E_{\mathrm{T},1} = 0.40\,\mathrm{eV}$ from the slope and a capture cross section $\sigma_{\mathrm{T},1} = 1.6 \times 10^{-14}\,\mathrm{cm^2}$ from the y-intercept.

Plotting the same data along the τ_Q axis in Fig. (3b) we can see the emission time constant $\tau_{\mathrm{E}1}$ of the trap reducing with increasing temperatures. Furthermore we observe a second peak with a time constant $\tau_\mathrm{X} \approx 20\,\mu$s with a weak temperature dependence. Because of this weak temperature dependence we do not interpret this time constant as an emission time of a second deep

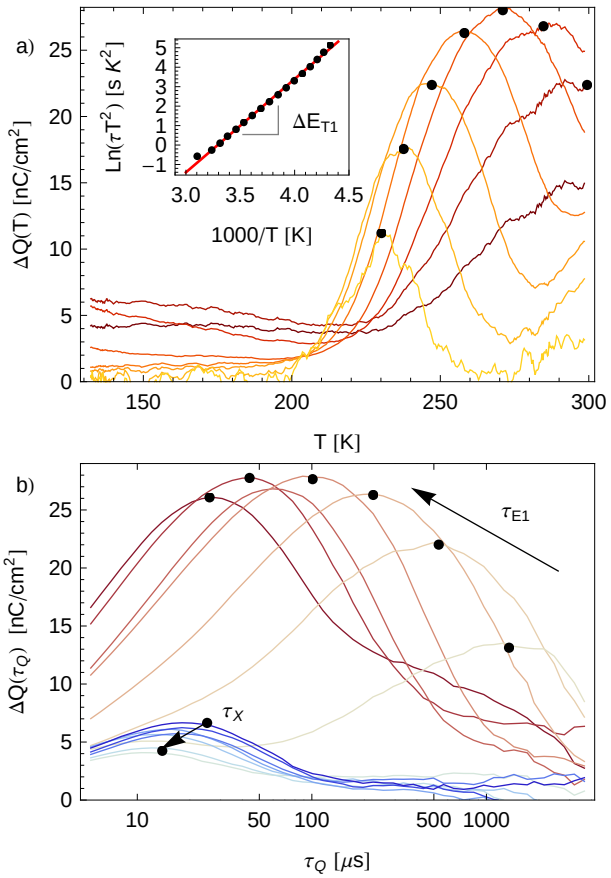

FIG. 3: **a)** DLTS spectrum (ΔQ) vs temperature (T) for different detector time constants (τ_Q). The Arrhenius plot in the inset relates the temperature at which the peak in ΔQ occurs and the corresponding τ_Q. The linear fit reveals an activation energy of $\Delta E_{\mathrm{T},1} = 0.40\,\mathrm{eV}$ and a crosssection $\sigma_{\mathrm{T},1} = 1.6 \times 10^{-14}\,\mathrm{cm^2}$. **b)** The same spectrum (ΔQ) as in (a) plotted vs. τ_Q for temperatures between 131 K (blue) and 300 K (red). The thermally activated emission time constant ($\tau_{\mathrm{E}1}$) is clearly visible. Additionally a weakly temperature dependent time constant $\tau_\mathrm{X} \approx 20\,\mu$s is present. This time constant is attributed to transport within the trap band.

trap state; instead, we attribute τ_X to a transport process with a low mobility, which can be estimated to be $d^2/(2\tau_\mathrm{X}V_\mathrm{D}) = 1.6 \times 10^{-6}\,\mathrm{cm^2/(Vs)}$. The total charge density in this process is $3 \times 10^{16}\,\mathrm{cm^{-3}}$ as determined from Fig. (2f).

Our DLTS measurements show clearly the presence of an abundant trap state with an activation energy of 0.40 eV, which we will refer to as the *T1 trap* for the rest of the discussion. However, the DLTS measurements do not determine whether carriers in the traps are thermally activated to the valence band or to the conduction band and whether the T1 trap is of acceptor or donor type. These questions are not straight forward to answer, because there is no consensus on the way charge is transported in NC solids, despite the fact that NC-based devices have existed for over 10 years. We will therefore discuss our findings in the context of two proposed models for band structure and charge transport in PbS NC solids: The model of a conventional p-type SC and the model recently proposed by Nagpal and Klimov based on

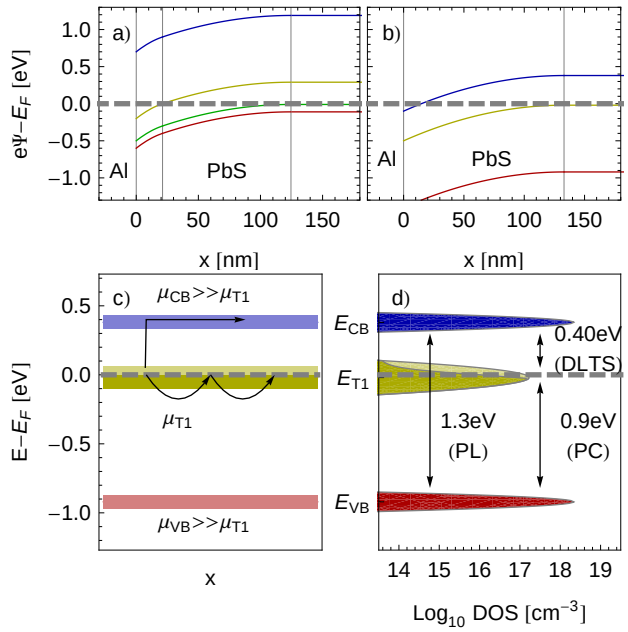

FIG. 4: **a)** Band diagram for the PbS:EDT/Al Schottky junction under the assumptions that the PbS NC solid is a conventional p-type SC (i.e. the Fermi energy is close to the VB (red) due to an intrinsic acceptor dopant (green)). In this picture the T1 trap (yellow) has to be of acceptor type and close to the VB. Within the space charge region (SCR), the Fermi energy crosses the T1 energy, which should be detectable by capacitance voltage measurements. **b)** Band diagram within the model of Nagpal [12], where the T1 trap (yellow) forms a metallic midgap band close to the CB (blue). The width and built-in voltage of the SCR are identical to the model considered in (a). **c)** The proposed band diagram for the PbS:EDT NC solid, based on the model in (b). The VB (red) and the CB (blue) are separated by the optical bandgap of the NCs (1.3 eV). The trap T1 (yellow) is located 0.4 eV below the CB and forms a band. DLTS measurements show emission of carriers from traps by thermal activation into the CB and direct hopping within the T1 band with a low mobility of $\mu_{T1} = 1.6 \times 10^{-6}\,\mathrm{cm}^2/(\mathrm{Vs})$. **d)** Our DLTS measurements further determine the density of states of the T1 band to be on the order of $1.7 \times 10^{17}\,\mathrm{cm}^{-3}$ with a small amount of free holes ($3 \times 10^{16}\,\mathrm{cm}^{-3}$) in the T1 band.

a metallic midgap band [12].

Before we start to discuss the specific models we want to clarify the fundamental assumptions that are commonly adopted in all models and are used in our calculations. Many reports on NC solids assume the existence of a conduction band (CB) and a valence band (VB) in a NC solid that derive directly from the lowest quantum confined states that are the source of the photoluminescence (PL) of individual NCs[8, 24, 25]. While this is a strong assumption, we adopt this view and terminology and define the distance between the VB and the CB as the optical bandgap; in the PbS NC used in this experiment we find $E_{VB} - E_{CB} = 1.3\,\mathrm{eV}$ by PL measurements shown in the Supplementary Information.

Moreover, for the calculation of the band alignment at the PbS/Al interface it is necessary to define the energy from the VB or CB to the vacuum level. As there is no consensus on the energy from the bands to the vacuum level we will use the Fermi energy as a fixed point in our model calculations. The Fermi energy (E_F) in PbS NC solids relative to the vacuum level was previously determined to be between $-4.7\,\mathrm{eV}$ [26] and $-4.9\,\mathrm{eV}$ [25, 27]. In a Schottky junction it is the difference of the Fermi energy to the metal workfunction (Ψ_{Al}) that is responsible for the built-in voltage and is given in first approximation by $qV_{bi} \approx \Psi_{Al} - E_F$. The measurement of an open circuit voltage of 0.47 V in our devices gives us an indication on the built-in voltage on the order of 0.5 V. This is in agreement with $E_F = -4.7\,\mathrm{eV}$, which we therefore use for our calculations.

The most popular model that is used in works on PbS NC solids is the one of a conventional p-type SC where E_F is close to the VB and conduction is mediated by holes in the VB [24, 27]. The density of intrinsic p-type dopants is usually found to be on the order of $3 \times 10^{16}\,\mathrm{cm}^{-3}$ and is often times attributed to oxygen or water related defects [28]. To be consistent with this model the T1 traps, which we observe by DLTS have to be of acceptor type and be located 0.4 eV above the VB. Using these assumptions we calculate the resulting Al/PbS junction band diagram in Fig. (4a) by solving Poissons equation. From the band diagram we find that a direct implication of this model is that the T1 level crosses the Fermi energy within the SCR. This crossing splits the SCR in two regions, which is a known phenomenon in the presence of large trap densities and should be detectable by frequency dependent capacitance-voltage measurements [17, 29].

A different model was recently put forward by Nagpal and Klimov based on photocurrent measurements in PbS NC FET structures [12]. They postulate the existence of a metallic midgap band to explain the conduction in the dark by low mobility carriers in this band. In contrast, photoconduction is related to high mobility carriers in the VB and possibly in the CB. They estimate that the midgap band is *nearly full* and is located 0.4 eV below the CB in agreement with earlier reports on photodetectors [30].

We can explain the observations in our DLTS measurements by identifying the T1 traps with the midgap band proposed by Nagpal. As shown in Fig. (4c) charge carriers can be transported by two different mechanisms. If temperatures are high enough, electrons can be thermally activated into the high mobility CB and are swept out quickly. This process is consistent with the observation of a thermally activated trap in our DLTS measurements and implies that the total density of states of the T1 band is on the order of $1.7 \times 10^{17}\,\mathrm{cm}^{-3}$.

Additionally, the model implies that carriers can move slowly within the T1 band without thermal activation. This agrees with our observation of a slow temperature independent transport process with a mobility on the order of $1.6 \times 10^{-6}\,\mathrm{cm}^2/(\mathrm{Vs})$, which we now attribute to transport within the T1 band. The free carrier density in the T1 band we observe is $3 \times 10^{16}\,\mathrm{cm}^{-3}$, which is compatible with previous measurements that had determined similar free hole densities [24]. While these carriers were assumed to be holes in the VB, in this model, we relate them to holes in the T1 band.

Fig. (4b) shows the expected band alignment for this model. While the band diagram and conduction mechanism is different in the two models, we find that the resulting SCR presents nearly identical to the first case in Fig. (4a) with a width of 125 nm and $V_{\mathrm{bi}} = 0.5\,\mathrm{V}$. This highlights why simple characterization methods like capacitance voltage or current voltage measurements are unlikely to discriminate between both models.

As the discussion shows above, current-based DLTS can help the understanding of charge transport significantly by contributing quantitative information on energies, time scales and carrier densities. In this study we were able to identify a deep trap level in a PbS:EDT NC solid with an activation energy of 0.40 eV and a density of $1.7\times10^{17}\,\mathrm{cm}^{-3}$ using only a minimum amount of assumptions to analyse the data. The experimental ease to get quantitative information on charge trapping using DLTS can help to test the effectiveness of chemical treatments to passivate electronic traps, which is necessary for rational design and improvement of materials and fabrication methods.

I. ACKNOWLEDGEMENTS

The authors thank Kevin McPeak and the OMEL at ETHZ for helpful discussions in the course of this work. Funding for this project was supported by the Swiss National Science Foundation (SNSF). TEM was performed at the Electron Microscopy ETH Zurich (EMEZ).

II. SUPPLEMENTARY INFORMATION

A. NC Synthesis and Characterization

The PbS NCs were made following Hines et al. [31] Octadecene (75 ml), lead (II) oxide (1.8 g), and oleic acid (5 ml) were mixed in the 250 ml four-neck flask. The mixture was dried under vacuum at 150 °C for 2 hours. During this time, the reaction solution slowly became colorless and transparent, indicating in-situ formation of Lead (II) oleate. Then the Lead (II) oleate solution was backfilled with the nitrogen. At temperature of 150 °C, 40 ml of 0.1 M solution of hexamethyldisilathiane in pre-purified octadecene was swiftly added. The reaction mixture was allowed to cool down to 100°C, after which this temperature was kept for another 5 min and then quenched with water bath. The PbS NCs were purified by standard solvent/nonsolvent procedure, using a hexane and acetone. The washing cycle was repeated 3 times. Lead (II) oxide (99.999 %) is purchased from Strem Chemicals; hexamethyldisilathiane (purum grade), octadecene (90 %, techn.), oleic acid (90 %), hexane, acetone, ethanol, toluene are from Sigma Aldrich. All chemicals were used as received. 3 nm-diameter PbS NCs used in this work. Transmission electron microscopy (TEM) and optical absorption data for the NCs are provided in Figure 1.

B. Device Fabrication

Devices were fabricated on cleaned, pre-patterned indium tin oxide (ITO) glass substrates from Thin Film technologies. The NC active layers were deposited using a multi-step dip-coating process. A home-built dip-coater sequentially immersed the patterned ITO substrate in a bath of NCs with concentration of 5 mg/ml in hexane, a bath of 2 mM ethanedithiol (EDT) in acetonitrile, and a rinse bath of acetonitrile. Wait times between each step of were selected to enable sufficient drying of the films between each immersion step. Repeating the processes 30 times resulted in a NC film thickness of $d = 67\,\mathrm{nm}$ determined by AFM. The top electrode consists of 1.5 nm of lithium fluoride (LiF), 100 nm aluminium, and 300 nm of silver thermally evaporated through a shadow mask. The additional layer of silver provides a robust and conductive electrode, which facilities measurements in the cryostat. An active device active area of $0.02\,\mathrm{cm}^2$ is defined by the overlap between the ITO and Al electrodes.

[1] J.-S. Lee, M. V. Kovalenko, J. Huang, D. S. Chung, and D. V. Talapin, Nature nanotechnology **6**, 348 (2011).
[2] D. S. Chung, J.-S. Lee, J. Huang, A. Nag, S. Ithurria, and D. V. Talapin, Nano letters **12**, 1813 (2012).
[3] J. Kwak, W. K. Bae, D. Lee, I. Park, J. Lim, M. Park, H. Cho, H. Woo, D. Y. Yoon, K. Char, et al., Nano letters **12**, 2362 (2012).
[4] W. Ma, J. M. Luther, H. Zheng, Y. Wu, and A. P. Alivisatos, Nano letters **9**, 1699 (2009).
[5] J. M. Luther, J. Gao, M. T. Lloyd, O. E. Semonin, M. C. Beard, and A. J. Nozik, Advanced Materials **80309**, n/a (2010).
[6] N. Zhao, T. P. Osedach, L.-Y. Chang, S. M. Geyer, D. Wanger, M. T. Binda, A. C. Arango, M. G. Bawendi, and V. Bulovic, ACS nano **4**, 3743 (2010).
[7] K. Szendrei, W. Gomulya, M. Yarema, W. Heiss, and M. A. Loi, Applied Physics Letters **97**, 203501 (2010).
[8] J. Gao, J. M. Luther, O. E. Semonin, R. J. Ellingson, A. J. Nozik, and M. C. Beard, Nano letters **11**, 1002 (2011).
[9] A. H. Ip, S. M. Thon, S. Hoogland, O. Voznyy, D. Zhitomirsky, R. Debnath, L. Levina, L. R. Rollny, G. H. Carey, A. Fischer, et al., Nature nanotechnology (2012).
[10] C. Sah, Solid-State Electronics **19**, 975 (1973).
[11] S. Sze and K. Ng, *Physics of semiconductor devices* (2006), ISBN 0471143235.
[12] P. Nagpal and V. I. Klimov, Nature Communications **2**, 486 (2011).
[13] J. Tang, K. W. Kemp, S. Hoogland, K. S. Jeong, H. Liu, L. Levina, M. Furukawa, X. Wang, R. Debnath, D. Cha, et al., Nature Materials (2011).
[14] K. Szendrei, M. Speirs, W. Gomulya, D. Jarzab, M. Manca, O. V. Mikhnenko, M. Yarema, B. J. Kooi, W. Heiss, and M. A. Loi, Advanced Functional Materials pp. n/a–n/a (2012).
[15] J. Gao and J. C. Johnson, ACS nano **6**, 3292 (2012).
[16] R. Loef, A. J. Houtepen, E. Talgorn, J. Schoonman, and A. Goossens, The Journal of Physical Chemistry C **113**,

15992 (2009).
[17] D. V. Lang, Topics in Applied Physics **37**, 93 (1979).
[18] O. Gaudin, R. B. Jackman, T.-P. Nguyen, and P. Le Rendu, Journal of Applied Physics **90**, 4196 (2001).
[19] J. Tang, X. Wang, L. Brzozowski, D. A. R. Barkhouse, R. Debnath, L. Levina, and E. H. Sargent, Advanced materials (Deerfield Beach, Fla.) **22**, 1398 (2010).
[20] D. V. Lang, Journal of Applied Physics **45**, 3023 (1974).
[21] J. Borsuk and R. Swanson, Electron Devices, IEEE Transactions ... **27**, 2217 (1980).
[22] C.-W. Lee, C. Renaud, C.-S. Hsu, and T.-P. Nguyen, Nanotechnology **19**, 455202 (2008).
[23] K. F. Cuff, M. R. Ellet, C. Kuglin, and L. Williams, in *7th In. Conf. Phys. Semicond.* (1964), p. 677.
[24] J. P. Clifford, K. W. Johnston, L. Levina, and E. H. Sargent, Applied Physics Letters **91**, 253117 (2007).
[25] B.-r. Hyun, Y.-w. Zhong, A. C. Bartnik, L. Sun, H. D. Abruña, F. W. Wise, J. D. Goodreau, J. R. Matthews, T. M. Leslie, and N. F. Borrelli, ACS nano **2**, 2206 (2008).
[26] P. Kulis, J. Butikova, B. Polyakov, G. Marcins, J. Pervenecka, K. Pudzs, and I. Tale, in *IOP Conference Series: Materials Science and Engineering* (2012), vol. 38, p. 012048.
[27] A. G. Pattantyus-Abraham, I. J. Kramer, A. R. Barkhouse, X. Wang, G. Konstantatos, R. Debnath, L. Levina, I. Raabe, M. K. Nazeeruddin, M. Grätzel, et al., ACS nano **4**, 3374 (2010).
[28] O. Voznyy, D. Zhitomirsky, P. Stadler, Z. Ning, S. Hoogland, and E. H. Sargent, ACS nano **6**, 8448 (2012).
[29] D. Taylor and H. Gomes, in *Electrical Insulation and Dielectric ...* (1995).
[30] G. Konstantatos and E. H. Sargent, Applied Physics Letters **91**, 173505 (2007).
[31] M. Hines and G. Scholes, Advanced Materials **15**, 1844 (2003).